Aging and Disease
www.aginganddisease.org
Early access date: March 23, 2026
http://dx.doi.org/10.14336/AD.2026.0063

Original Article

SIRT2 Delays Vulnerable Plaque Progression by Modulating Vascular Smooth Muscle Cell Senescence

Leli Zhang[1#], Pengrong Guo [1], Yue Wang[1], Zhenbai Qin[1], Yi Zou[1], Wenxin Zhao[1], Xiaofan Wu[1*]

[1]Department of Cardiology, Beijing Anzhen Hospital, Capital Medical University, Beijing, China

[Received January 16, 2026; Revised March 19, 2026; Accepted March 20, 2026]

ABSTRACT: The rupture of vulnerable plaques (VPs) serves as the pathophysiological foundation for the occurrence of acute coronary syndrome (ACS). The senescence of vascular smooth muscle cells (VSMCs) is pivotal in the formation and even rupture of VPs. Although previous studies have demonstrated that Sirt2 contributes to the attenuation of vascular aging, its specific mechanisms in VSMC senescence and vulnerable plaque formation remain poorly understood. This study aimed to explore the underlying mechanism of Sirt2 in the formation of vulnerable plaques. Male ApoE$^{-/-}$ mice were randomly divided into three groups and administered normal saline, empty vector AAV9, or VSMC-specific Sirt2-overexpressing AAV9 via tail vein injection, respectively. Four weeks after viral infection, a mouse model of vulnerable carotid plaques was established by partial ligation of the left carotid artery combined with 8 weeks of high-fat diet feeding. We found that VSMC-specific Sirt2 overexpression significantly delayed VSMC senescence and VP formation. Furthermore, after Sirt2 overexpression, the phosphorylation levels of AMPK and FOXO3a in VSMCs were increased considerably. In vitro further verified that Sirt2 reverses H_2O_2-induced VSMC senescence via the AMPK/FOXO3a pathway. Additionally, using resveratrol, we demonstrated that its protective effects against VSMC senescence are mediated through the Sirt2-AMPK-FOXO3a axis. In conclusion, our experimental data suggest that Sirt2 delays VSMC senescence potentially through the AMPK/FOXO3a pathway, thereby attenuating VPs formation. This study highlights Sirt2 as a potential therapeutic target, and pharmacological activation of Sirt2 may represent a promising strategy for delaying VPs formation and preventing ACS.

Keywords: Sirt2, atherosclerosis, vulnerable plaque, aging, vascular smooth muscle cell senescence

INTRODUCTION

Although substantial advancements have been made in the diagnosis and treatment of acute coronary syndrome (ACS), ACS still ranks as one of the crucial causes of acute cardiovascular death [1]. The primary pathophysiological foundation of ACS is the rupture of vulnerable plaques (VPs). The main characteristics of VPs are a large and well-developed necrotic core, along with a thin fibrous cap (≤65 μm) [2]. Plaque stability is predominantly determined by the thickness of the fibrous cap and the size of the necrotic core [3]. The fibrous cap is constituted by vascular smooth muscle cells (VSMCs) and extracellular matrix (ECM) components, including collagen, elastin, and proteoglycans. Senescent VSMCs undergo a shift toward a senescence-associated secretory phenotype (SASP), characterized by the secretion of large amounts of pro-inflammatory cytokines, chemokines, and matrix metalloproteinases (MMPs). Among these, MMPs degrade ECM components such as collagen fibers, leading to thinning of the fibrous cap and thereby promoting VPs formation and rupture [4]. Therefore, identifying genetic regulators of VSMC senescence and elucidating the associated molecular mechanisms constitute a critical strategy for inhibiting VP progression and ACS.

Sirtuins (SIRTs), a family of NAD^+-dependent deacetylases, play pivotal roles in a multitude of

***Correspondence should be addressed to:** Dr. Xiaofan Wu, Department of Cardiology, Beijing Anzhen Hospital, Capital Medical University, Beijing, China. Email: drwuxf@163.com. #First author.

physiological and pathological processes within the human body, including aging, apoptosis, inflammation, and biological rhythms [5]. Zhang et al. analyzed the transcriptomic data of 604 human aortas from the Genotype-Tissue Expression (GTEx) database and found that SIRT2 is the member of the Sirtuin family with the highest basal expression level in the human aorta, suggesting that SIRT2 may play a significant role in vascular physiology [6]. However, compared to SIRT1, SIRT3, and SIRT6, research on the function of SIRT2 in cardiovascular aging remains relatively limited [7]. In recent years, studies by Tang et al. and Ye et al. have successively revealed the role of SIRT2 in myocardial aging [8, 9]. Furthermore, Zhang et al. found that the expression level of Sirt2 in aortic VSMCs of aging mice was significantly lower than that in young mice, and that Sirt2 deficiency exacerbated aging-induced vascular stiffness [6]. Although several studies have uncovered the associations between SIRT2 and age-related vascular disorders, the role of SIRT2 in the senescence of VSMCs and the development of VPs warrants further investigation.

AMP-activated protein kinase (AMPK), a cellular energy sensor, plays a critical role in regulating various physiological and pathological processes, including metabolic disorders, cancer, and aging [10]. Tang et al. demonstrated that SIRT2 can activate AMPK and thereby delay aging-associated cardiac hypertrophy [8]. FOXO3, a transcription factor, contributes significantly to anti-aging mechanisms by coordinating key biological processes such as antioxidant defense and anti-inflammatory responses [11]. Xia et al. reported that macrophage migration inhibitory factor (MIF) restores the viability of senescent mesenchymal stem cells (MSCs) through activation of the AMPK-FOXO3a signaling pathway [12]. However, the involvement of the AMPK-FOXO3a signaling pathway in VSMC senescence remains unclear.

In this study, we utilized a mouse model of vulnerable plaque to investigate the impact of Sirt2 overexpression on plaque stability. Furthermore, we elucidated the role of Sirt2 in VSMC senescence both in vitro and in vivo. Notably, we found that inhibition of AMPK abolishes the protective effect of Sirt2 against H2O2-induced VSMC senescence. Finally, we further confirmed in vitro that the protective effects of resveratrol against VSMC senescence are mediated through the Sirt2-AMPK-FOXO3a pathway. These findings not only validate Sirt2 as a key regulator of VSMC senescence but also highlight its potential as a therapeutic target. Pharmacological activation of Sirt2, such as with resveratrol, may represent a promising strategy for enhancing plaque stability and preventing ACS.

MATERIALS AND METHODS

Experimental animals

All animal procedures were approved by the Institutional Animal Care and Use Committee of Capital Medical University and conformed to the National Institutes of Health Guide for the Care and Use of Laboratory Animals.

Three-week-old male ApoE$^{-/-}$ mice were obtained from Beijing Huafukang Biotechnology Co., Ltd. (Beijing, China). Following a one-week acclimatization period under specific pathogen-free (SPF) conditions, the 4-week-old mice were randomly divided into three groups (n = 6 per group): (1) Vehicle group (injected with an equal volume of PBS); (2) AAV-NC group (injected with serotype 9 adeno-associated virus (AAV9)-empty vector); (3) AAV-Sirt2 group (injected with AAV9-Sirt2, an AAV9 virus carrying the Sm22α promoter and a Sirt2 overexpression sequence targeting VSMCs). All viral vectors were constructed and packaged by Shanghai GeneChem Co., Ltd. (Shanghai, China). The viral stocks were diluted in PBS to a final titer of 5×10^{12} viral genomes (vg)/mL, and a volume of 200 μL (corresponding to a total dose of 1×10^{12} vg per mouse) was delivered via intravenous tail vein injection. At four weeks post-viral injection, we harvested mouse arteries for preliminary assessment of transfection efficiency via reverse transcription polymerase chain reaction (RT-PCR) and western blot (Supplementary Fig. 2A). To validate the VSMC-specificity of Sirt2 overexpression, we performed co-staining for Sirt2 with the VSMC marker α-SMA, as well as with the macrophage marker CD68 and the endothelial cell marker CD31 (Supplementary Fig. 2B-D).

Four weeks post-injection (at 8 weeks of age), all mice underwent partial ligation of the left common carotid artery (LCCA) to induce the formation of vulnerable atherosclerotic plaques. Briefly, anesthesia was induced by intraperitoneal administration of 1% sodium pentobarbital (50 mg/kg). The mice were then positioned on a heating pad maintained at 37°C. A cervical incision was made, followed by blunt dissection to expose the LCCA and its branches. The internal and external carotid arteries were permanently ligated with 6-0 surgical sutures, while the superior thyroid artery was preserved. Immediately after surgery, all animals were placed on a high-fat diet (21% fat, 0.15% cholesterol, 4 kcal/g) for 8 weeks.

Ultrasound imaging

To evaluate plaque formation and stability following partial ligation of the left common carotid artery (LCCA),

ultrasound examination of the mouse LCCA was performed 8 weeks after the ligation surgery. After anesthesia induction with 2% isoflurane inhalation, the neck hair of the mice was removed, and the animals were properly secured. The examination table was tilted approximately 30° to the left so that the ultrasound probe remained parallel to the long axis of the mouse's body with slight lateral inclination. After applying coupling gel to the neck area, the left common carotid artery was scanned along its long axis using the anterolateral surface of the probe. The following parameters were observed and recorded: intima-media thickness (IMT), eccentric index (EI), maximum blood flow velocity (Vmax), as well as morphological features such as plaque rupture and intraplaque hemorrhage. The eccentric index was calculated as: EI = (maximum IMT − minimum IMT) / maximum IMT.

Specimen collection

Following carotid ultrasound examination, all mice were fasted (with free access to water) for 12 hours and then anesthetized by intraperitoneal injection of 1% sodium pentobarbital. After anesthesia was confirmed, the thoracic and abdominal skin was disinfected with 75% ethanol. The thoracic cavity was quickly opened, and the diaphragm was incised to fully expose the heart. Blood was collected from the left ventricle. The right atrium was then opened, and the left ventricle was cannulated for rapid perfusion with heparinized (1%) saline until the liver turned pale and the effluent from the right atrium became clear, ensuring thorough removal of residual blood from the vasculature. Subsequently, the left common carotid artery was carefully dissected and divided into two segments for further processing. One-half of the tissue was immediately placed in 4% paraformaldehyde and fixed at 4°C for 24 hours. The other half was directly embedded in OCT compound and stored at –20°C for future use.

Histopathological and immunohistochemical/ immunofluorescence Staining

Paraffin-embedded sections (5 μm thick) of the mouse left common carotid artery were used for hematoxylin-eosin (HE) staining and Masson's trichrome staining, while frozen sections (7 μm thick) were used for Oil Red O staining.

Immunohistochemical (IHC) and immunofluorescence (IF) staining were performed using paraffin sections and frozen sections, respectively. After blocking with 5% bovine serum albumin (BSA), the sections were incubated overnight at 4°C with the following primary antibodies diluted in blocking buffer: anti-α-SMA (α-smooth muscle actin) (Abcam, ab7817, 1:200), anti-CD68 (Signalway Antibody, #38005, 1:200), anti-CD31 (Signalway Antibody, #29555, 1:200), anti-IL-1β (Abcam, ab283818, 1:500), anti-TNF-α (Abcam, ab307164, 1:1000), anti-MMP2 (Abcam, ab86607, 1:200), anti-Sirt2 (Signalway Antibody, #32057, 1:200), anti-$p16^{INK4a}$ (Signalway Antibody, #62008, 1:200), anti-p21 (Signalway Antibody, #41297, 1:200), anti-phospho-AMPK (Signalway Antibody, #14099, 1:200), and anti-phospho-FOXO3a (Signalway Antibody, #12199, 1:500). To validate antibody specificity, secondary-only controls (primary antibody omitted) were included to assess non-specific binding. All control sections were processed identically to the experimental samples. The following day, the sections were incubated with appropriate secondary antibodies (IHC: ZSGB-BIO, PV-6001, PV-6002; IF: Servicebio, GB21303, GB25301, 1:300). Control sections were incubated with the same secondary antibodies. Nuclei were counterstained with DAPI or hematoxylin. Finally, images were captured using a fluorescence microscope (ECLIPSE Ni, Nikon, Japan). Subsequent image processing and analysis were performed using ImageJ software (National Institutes of Health, Bethesda, MD, USA).

Senescence β-galactosidase staining (SA-β-gal Staining)

Frozen sections of the mouse LCCA or primary VSMCs cultured in 24-well plates were stained using a Senescence β-Galactosidase Staining Kit (Sigma, #CS0030-1KT, USA) according to the manufacturer's instructions. Briefly, samples were fixed with the provided fixation buffer for 15 min at room temperature, then rinsed with PBS. The staining working solution was freshly prepared by mixing the following components according to the manufacturer's protocol: 10μL of β-galactosidase staining solution A, 10μL of staining solution B, 930μL of staining solution C, and 50μL of X-Gal solution. The samples were incubated with the staining working solution at 37°C without CO_2 in the dark overnight. The next day, after observing blue-green staining under a light microscope, the reaction was stopped by washing with PBS.

For mouse carotid arteries, immunohistochemical staining was further performed to determine the proportion of senescent cells in vascular smooth muscle cells. The sections were incubated overnight with anti-α-SMA (Abcam, ab7817, 1:200), followed by counterstaining with hematoxylin.

Isolation of primary vascular smooth muscle cells

Four-week-old male C57BL/6 mice (Beijing Huafukang Biotechnology, Beijing, China) were anesthetized by

intraperitoneal injection of 1% sodium pentobarbital. After thoracotomy, lung tissue was excised along the hilum, and the aorta was dissected along the spinal column, then placed in calcium- and magnesium-containing Hanks' balanced salt solution (HBSS) (Solarbio, H1025, Beijing, China). Under a sterile laminar flow hood, perivascular fat and connective tissue were carefully removed from the aorta under a microscope. The vessel was cut longitudinally and transferred to a solution containing collagenase type I for digestion at 37 °C for 15 min. Subsequently, the tissue was cut into approximately 1 mm² pieces and attached to a pre-scratched "#"-pattern in a 6-well plate. A small amount of sterilized silicone grease was applied to a coverslip, which was then placed over the tissue fragments. Gentle tapping excluded air between the coverslip and the tissue. The wells were then filled with Dulbecco's modified Eagle medium (DMEM, Sigma, USA) supplemented with 20% fetal bovine serum (FBS, Gibco, USA). Cultures were maintained in a 37 °C, 5% CO_2 incubator, with medium changes every 3 days. Primary cells were passaged approximately 7 days later for subsequent experiments.

Establishment of mouse VSMCs stably overexpressing Sirt2

To generate a stable cell line overexpressing Sirt2, primary VSMCs were infected with pLVX-mSirt2-3xFLAG-ZsGreenPuro (NM_022432.5) (Hanbio Biotechnology Co., Shanghai, China; titer: 1×10^8 TU/mL). Cells were seeded at 30–40% confluence and infected at a multiplicity of infection (MOI) of 30 in the presence of 5 μg/mL Polybrene. After 24 h, the medium was replaced with fresh complete medium. Seventy-two hours post-infection, selection was performed using medium containing 3 μg/mL puromycin to obtain stable clones. Cells infected with an empty vector were used as controls. Overexpression efficiency was confirmed by RT-PCR and Western blot analysis (Supplementary Fig. 3).

Establishment and Grouping of Cellular Senescence Models

Primary VSMCs were treated with increasing concentrations of H_2O_2 (0, 1, 10, 50, 100 μM; Sigma, Catalog No. 7722-84-1, USA) for 72 hours to induce senescence. SA-β-gal staining was performed to assess senescence, and the optimal concentration for inducing senescence without triggering cell death was determined (Supplementary Fig. 4A). To exclude potential confounding effects of apoptosis or ferroptosis, expression of Cleaved Caspase-3 and GPX4 was examined by Western blot (Supplementary Fig. 4B). Based on these validation experiments, treatment with 10 μM H_2O_2 for 72 hours was selected for establishing the VSMC senescence model in all subsequent experiments.

To investigate the role and potential mechanism of Sirt2 in VSMC senescence, the VSMCs were divided into the following six groups: (1) Control group; (2) H_2O_2 group: treated with 10 μM H_2O_2 for 72 hours; (3) AGK2 group: treated with 10 μM H_2O_2 and 10 μM AGK2 (a selective Sirt2 inhibitor, MCE, HY-100578, USA) for 72 hours; (4) LV-NC group: VSMCs infected with empty lentivirus to obtain stable transfectants, then treated with 10 μM H_2O_2 for 72 hours; (5) LV-Sirt2 group: VSMCs stably overexpressing Sirt2 treated with 10 μM H_2O_2 for 72 hours; (6) BAY-3827 group: VSMCs stably overexpressing Sirt2 treated with 10 μM H_2O_2 and 10 nM BAY-3827 (a selective AMPK inhibitor, MCE, HY-112083, USA) for 72 hours.

To investigate the potential of Sirt2-targeting agents in VSMC senescence, we performed experiments using resveratrol (MCE, HY-16561, USA). Based on previous reports demonstrating that 50 μM resveratrol exerts effective biological activity without inducing apoptosis [13, 14], VSMCs were divided into the following three groups: (1) H_2O_2 group: treated with 10 μM H_2O_2 for 72 hours; (2) RESV group: co-treated with 50 μM resveratrol and 10 μM H_2O_2 for 72 hours; (3) RESV+AGK2 group: co-treated with 50 μM resveratrol, 10 μM H_2O_2, and 10 μM AGK2 for 72 hours.

Reverse transcription polymerase chain reaction

Total RNA was extracted from cell or tissue samples using Trizol reagent (Invitrogen, USA), followed by phase separation with chloroform, precipitation with isopropanol, and washing with RNase-free 75% ethanol. RNA concentration was measured using a NanoDrop spectrophotometer (Thermo Scientific, USA), and RNA purity was assessed based on the A260/A280 ratio (ideal range 1.9–2.1) and A260/A230 ratio (>2.0). First-strand cDNA was synthesized from 1 μg of total RNA using a reverse transcription kit (RR047A, Takara, Japan). Real-time quantitative polymerase chain reaction (PCR) was performed on an iCycler iQ system (Bio-Rad, USA) using SYBR Green Master Mix (RR820A, Takara, Japan). The PCR protocol consisted of enzyme activation at 95°C for 30 s, followed by 40 cycles of denaturation at 95°C for 5 s and annealing/extension at 60°C for 30 s, with a final step of 95°C for 10 s and 60°C for 5 s after the last cycle. Each sample was run in three technical replicates, and mRNA expression levels were normalized to the housekeeping gene GAPDH. Relative changes in mRNA expression were analyzed using the $2^{-\Delta\Delta Ct}$ method. The primer sequences for mSirt2 were as follows: forward, 5'-

AGCCAACCATCTGCCACTAC-3'; reverse, 5'-CCAGC CCATCGTGTATTCTT-3'.

Western blotting analysis

Total protein was extracted using RIPA lysis buffer (APPLYGEN, C1053, Beijing, China) and quantified using the BCA method. Samples containing 15–30 μg of protein from each group were loaded for SDS-PAGE electrophoresis. After electrophoresis, proteins were transferred onto a PVDF membrane, which was then blocked with 5% skim milk for 1 hour. Following blocking, the membrane was incubated overnight at 4°C with primary antibodies specific to the target proteins. The primary antibodies used were as follows: anti-sirt2 (Proteintech, Cat No. 19655-1-AP, 1:10000); anti-$p16^{INK4a}$ (Abcam, #ab211542, 1:2000); anti-p21 (Abcam, #ab109199, 1:1000); anti-AMPK (Cell Signaling Technology, #5831, 1:1000); anti-FOXO3a (Cell Signaling Technology, #12829, 1:1000); anti-phospho-AMPK (Cell Signaling Technology, #4188, 1:2000); anti-phospho-FOXO3a (Cell Signaling Technology, #8174, 1:1000); anti-Cleaved Caspase-3 (Cell Signaling Technology, #9661, 1:1000); anti-GPX4 (Cell Signaling Technology, #52455, 1:1000); anti-β-actin (Servicebio, GB15003, 1:1000). The next day, unbound primary antibodies were thoroughly washed off with TBST, and the membrane was incubated with corresponding fluorescently labeled secondary antibodies (LI-COR Biosciences, 926-32211, USA) at room temperature for 1 hour. Scanning was performed using the Odyssey infrared imaging system (LI-COR Biosciences, Lincoln, USA). Finally, band positions and intensities were analyzed using ImageJ software (National Institutes of Health, Bethesda, MD, USA). Relative protein expression was determined by normalizing target band intensity to β-actin, followed by normalization to the mean value of the respective control group (set to 1) as specified in each figure legend.

Enzyme-Linked Immunosorbent Assay (ELISA)

The concentrations of SASP factors—TNF-α (Shanghai Enzyme-linked Biotechnology, ml002095, China), IL-6β (Shanghai Enzyme-linked Biotechnology, ml098416, China), and MMP-2 (Shanghai Enzyme-linked Biotechnology, ml106747, China)—were measured using mouse ELISA detection kits according to the manufacturer's instructions. Briefly, cell culture supernatants were collected, centrifuged at 1,000 × g for 10 min at 4°C. For each assay, 100μL of standard or sample was added to pre-coated plates and incubated for 90 min at 37°C. After washing, 100μL of biotinylated detection antibody was added and incubated for 60 min at 37°C, followed by 100μL of HRP-conjugated streptavidin for 30 min at 37°C in the dark. After five washes, 100μL of TMB substrate was added and incubated for 15 min at 37°C in the dark. The reaction was stopped with 50μL of 2 M H_2SO_4, and absorbance was measured at 450 nm using a ReadMax 1900 full-wavelength microplate reader (Shanpu Technology Co., Ltd., Beijing, China). Standard curves were generated using serial dilutions of the provided standards, and sample concentrations were calculated by interpolating optical density values from the standard curves. The units for all measured cytokines are expressed as pg/mL. All samples were set up in duplicate, and the experiment was independently repeated three times.

Statistical analysis

Statistical analyses were performed using GraphPad Prism 9.5(GraphPad Software, USA). All experiments were performed with at least three technical replicates, and the number of biological replicates for each experiment is specified in the corresponding figure legends. Data are presented as mean ± standard deviation (SD). Normality was assessed with the Shapiro-Wilk test. Normally distributed data were analyzed using an unpaired two-tailed t-test (two groups) or one-way ANOVA followed by Holm-Šidák's post hoc test (≥3 groups). Non-normally distributed data were analyzed using nonparametric tests, specifically the Mann-Whitney U test (two groups) or the Kruskal-Wallis test followed by Dunn's post hoc test (≥3 groups). Multiple comparisons across outcome measures were corrected via the Benjamini–Hochberg false discovery rate procedure. A p-value or adjusted p-value <0.05 was considered significant.

RESULTS

Sirt2 attenuates the formation of VPs in the mouse carotid artery

In our preliminary study, we evaluated a mouse model of vulnerable plaques. Twelve 8-week-old $ApoE^{-/-}$ mice were divided into a sham group and a vehicle group. They underwent sham surgery or partial left carotid artery ligation, respectively. Eight weeks after surgery, ultrasound examination of the left carotid artery revealed a significant increase in intima-media thickness and eccentricity index in the model group, along with apparent plaque formation, indicating successful establishment of the vulnerable plaque model (Supplementary Fig. 1).

Previous analyses of both the human aorta GTEx database and mouse aortic bulk RNA-seq have shown that SIRT2 is the member of the Sirtuin family with the

highest basal expression level. Furthermore, Sirt2 expression levels were significantly reduced in aortic VSMCs of aged mice [6], suggesting that Sirt2 in VSMCs may be involved in the process of vascular aging.

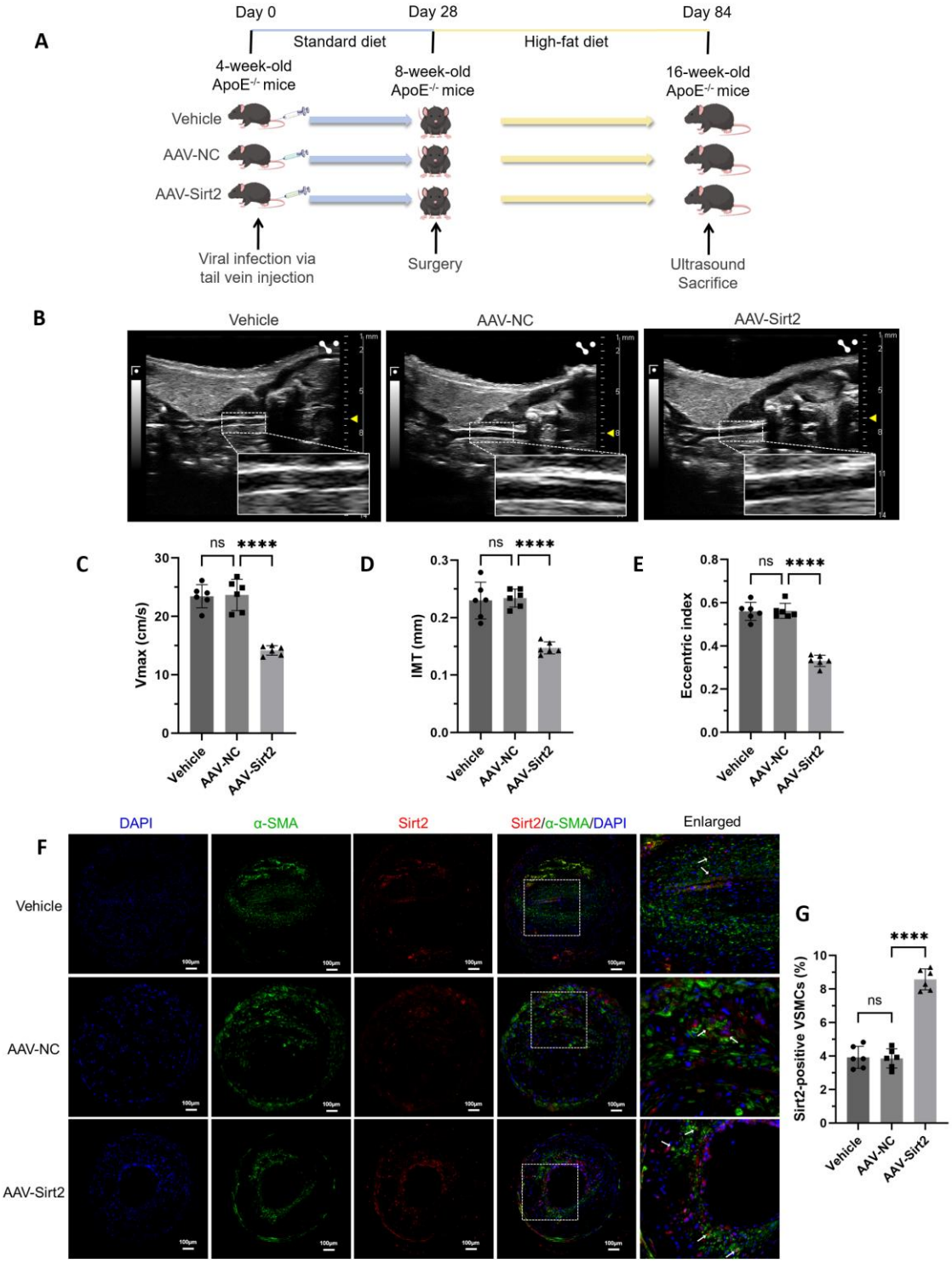

Figure 1. Sirt2 Delays the Formation of Vulnerable Plaques in ApoE$^{-/-}$ Mice. (A) Experimental timeline. **(B)** Representative long-axis micro-ultrasound images of the left common carotid artery. **(C-E)** Quantification of Vmax (C), IMT (D), and EI (E). **(F)** Immunofluorescence images showing Sirt2 (red) and α-SMA (green) co-localization. Arrows indicate Sirt2-positive VSMCs. **(G)** Quantification of Sirt2 expression in VSMCs. Scale bar = 100 μm. All data were analyzed by one-way ANOVA with Holm-Šídák's post hoc test. Note: n=6 mice per group; ns: not significant; *P< 0.05; **P< 0.01; ***P< 0.001; ****P< 0.0001.

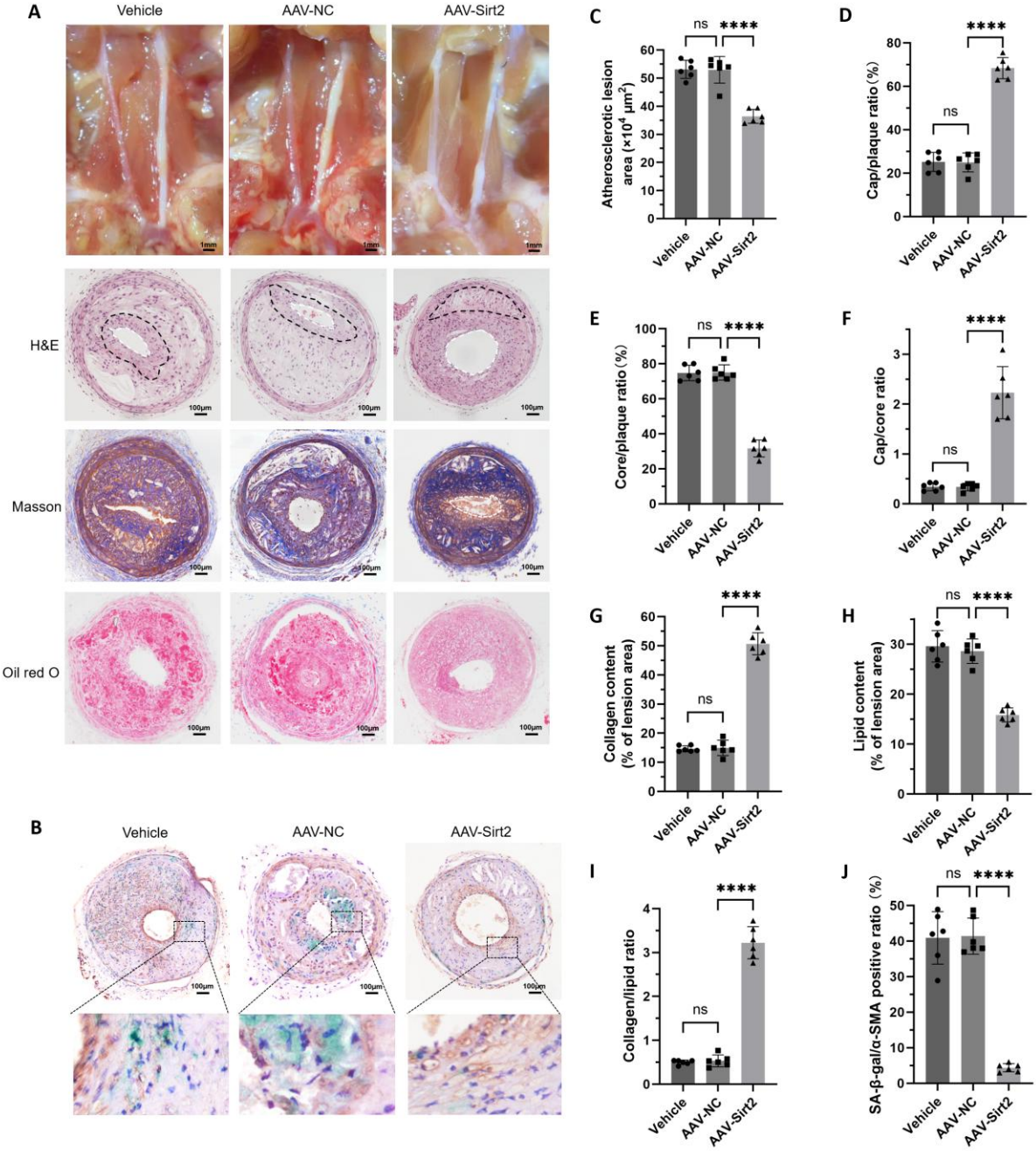

Figure 2. Effects of Sirt2 on Vulnerable Plaques and VSMCs in Mice. (A) Representative micrographs of the common carotid artery and cross-sectional slices stained with H&E, Masson's trichrome, and Oil Red O. In H&E staining, black dashed lines outline the fibrous cap (vehicle and AAV-NC groups) or lipid infiltration area (AAV-Sirt2 group); white dashed lines indicate the lumen. **(B)** Representative images of SA-β-gal staining (blue) and α-SMA immunohistochemistry (brown). Blue: senescent cells; brown: VSMCs; co-localization indicates senescent VSMCs. **(C-I)** Quantification of atherosclerotic lesion area (C), fibrous cap area/plaque area (D), lipid core area/plaque area (E), fibrous cap/lipid core ratio (F), collagen content (G), lipid content (H), and collagen/lipid ratio (I). **(J)** Quantification of senescent VSMCs. Scale bars: 1 mm (A, top), 100 μm (A, rows 2-4; B). All data were analyzed by one-way ANOVA with Holm-Šídák's post hoc test. Note: n=6 mice per group; ns: not significant; **P*< 0.05; ***P*< 0.01; ****P*< 0.001; *****P*< 0.0001.

Therefore, to clarify the role of Sirt2 in VSMC senescence and VPs, we randomly divided 18 four-week-old male ApoE$^{-/-}$ mice into three groups: a vehicle group, an AAV-NC group, and an AAV-Sirt2 group. These groups received tail vein injections of equal volumes of PBS, empty AAV9, or AAV9 carrying a Sirt2

overexpression sequence, respectively. After four weeks of viral infection, the mice (8 weeks old) underwent partial left carotid artery ligation, followed by eight weeks of high-fat diet feeding. Ultrasound examination was performed when the mice reached 16 weeks of age, followed by the collection of the left carotid artery (Fig. 1A).

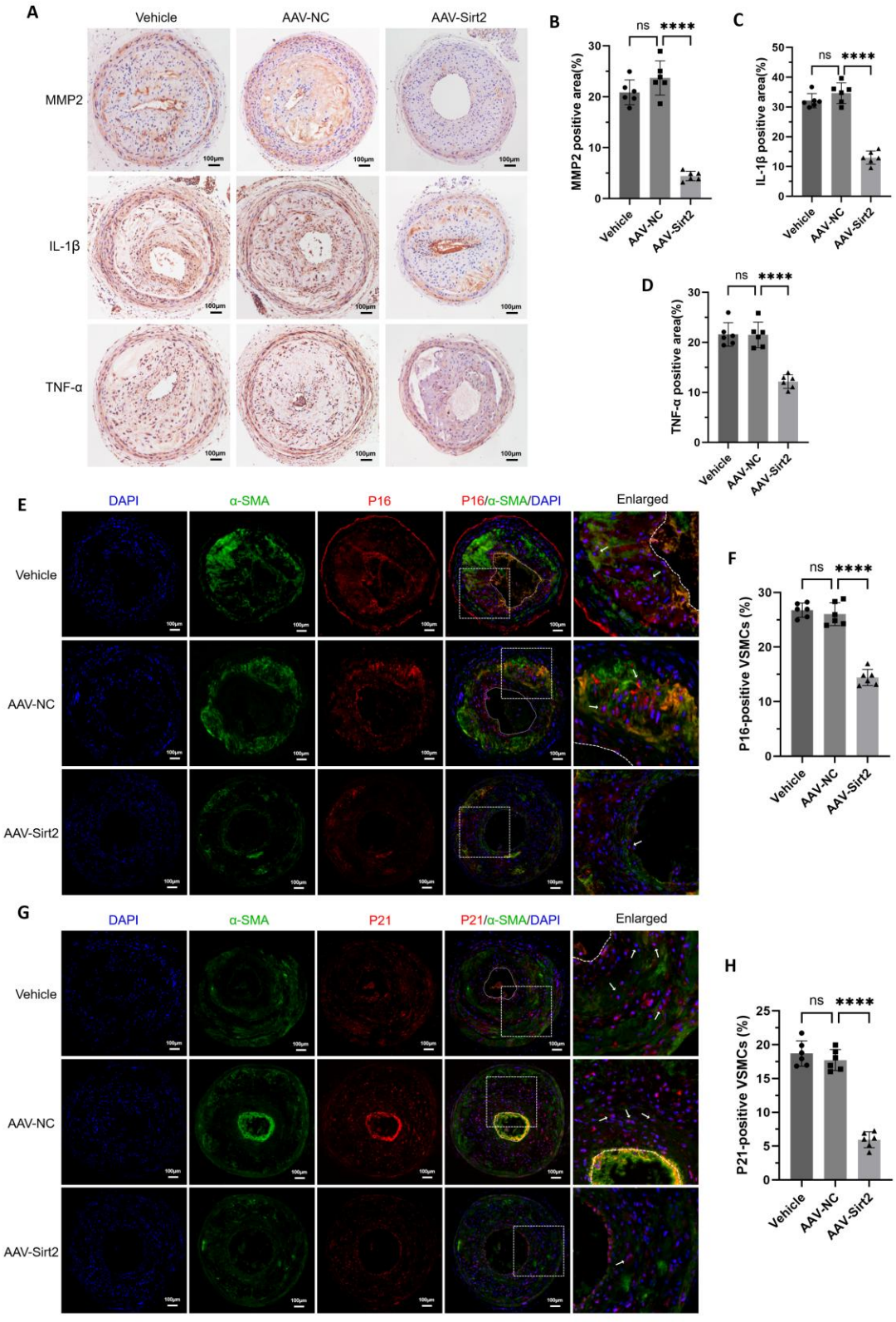

Figure 3. Effects of Sirt2 on the SASPs and senescence markers in VSMCs within VPs. (A) Representative immunohistochemical staining of MMP-2, IL-1β, and TNF-α. Scale bar = 100 μm. (**B-D)** Quantification of MMP-2 (B), IL-1β (C), and TNF-α (D) positive area as a percentage of total plaque area. **(E)** Immunofluorescence images showing P16 (red) and α-SMA (green) co-localization. Arrows indicate P16-positive VSMCs. Scale bar = 100 μm. **(F)** Quantification of P16 expression in VSMCs. **(G)** Immunofluorescence images showing P21 (red) and α-SMA (green) co-localization. Arrows indicate P21-positive VSMCs. Scale bar = 100 μm. **(H)** Quantification of P21 expression in VSMCs. All data were analyzed by one-way ANOVA with Holm-Šídák's post hoc test. Note: n=6 mice per group; ns: not significant; **P*< 0.05; ***P*< 0.01; ****P*< 0.001; *****P*< 0.0001.

Immunofluorescence double staining of the harvested left carotid arteries showed that Sirt2 expression was significantly higher in the AAV-Sirt2 group compared to the vehicle and AAV-NC groups (Fig. 1F-G). To validate the VSMC-specificity of Sirt2 overexpression, we further examined Sirt2 expression in macrophages and endothelial cells. No significant differences in Sirt2 expression were observed in CD68-positive macrophages or CD31-positive endothelial cells between groups, confirming that the SM22α promoter-driven Sirt2 overexpression was specifically restricted to VSMCs (Supplementary Fig.2C-D).

Analysis of carotid ultrasound images revealed markedly reduced V max, IMT, and EI in the AAV-Sirt2 group (Fig. 1B-E). Pathological staining results indicated a significant decrease in total plaque area, core-to-plaque size and intra-plaque lipid content in the AAV-Sirt2 group (Fig. 2A, C, E, H). In contrast, the fibrous cap area as a proportion of total plaque, the fibrous cap-to-lipid core ratio, intra-plaque collagen content, and the collagen-to-lipid ratio within plaques were significantly increased compared to the vehicle and AAV-NC groups (Fig. 2A, D, F, G, I). These findings suggest that Sirt2 enhances the stability of atherosclerotic plaques and slows the formation of VPs.

Sirt2 Delays Senescence of VSMCs in VPs

Senescent VSMCs play a crucial role in the formation and rupture of vulnerable plaques (VPs). To clarify the effect of Sirt2 on VSMC senescence within mouse carotid artery plaques, we assessed VSMC senescence in the VPs using SA-β-gal senescence staining combined with α-SMA immunohistochemical staining. Furthermore, we detected common SASP factors via immunohistochemical staining and examined the classical senescence markers cyclin-dependent kinase inhibitor 2A ($P16^{INK4A}$) and cyclin-dependent kinase inhibitor 1 (P21) in VSMCs using immunofluorescence double staining.

Our results demonstrated that in the AAV-Sirt2 group, the proportion of senescent VSMCs (Fig. 2B, J) and the levels of common SASP factors (MMP-2, IL-1β, TNF-α) within the plaques were significantly reduced (Fig. 3A-D). Additionally, the expression of senescence markers $P16^{INK4A}$ and P21 in VSMCs was markedly lower compared to the vehicle and AAV-NC groups (Fig. 3E-H). These findings suggest that Sirt2 significantly delays the senescence of VSMCs in VPs.

Sirt2 Delays Senescence in Primary VSMCs

Subsequently, to investigate the role of Sirt2 in primary VSMC senescence, we first established an in vitro senescence model. Dose-response experiments showed that 10 μM H_2O_2 for 72 hours optimally induced VSMC senescence without triggering apoptosis or ferroptosis, as confirmed by SA-β-gal staining and the absence of changes in Cleaved Caspase-3 and GPX4 expression (Supplementary Fig. 4). To clarify the function of Sirt2, we constructed Sirt2-overexpressing VSMCs via lentiviral infection and further validated the findings by applying the specific Sirt2 inhibitor AGK2. Senescence in primary VSMCs was assessed using SA-β-gal staining. The levels of SASP factors were measured by ELISA, and the expression of the VSMC senescence markers $P16^{INK4A}$ and P21 was evaluated by western blot.

After treatment with 10 μM H_2O_2 for 72 hours, the expression level of Sirt2 in primary VSMCs was significantly decreased compared to the control group (Fig. 4C-D). Concurrently, the number of senescent VSMCs (Fig. 4 A-B), the levels of senescence markers $P16^{INK4A}$ and P21 (Fig. 4C, E, F), and the SASP factors including MMP2, IL-1β, and TNF-α were significantly increased (Fig. 4L-N). Treatment with the Sirt2-specific inhibitor AGK2 further exacerbated the degree of VSMC senescence (Fig. 4A-F, L-N). Conversely, overexpression of Sirt2 led to a significant reduction in the number of senescent VSMCs (Fig. 4G-H), as well as the levels of $P16^{INK4A}$, P21 (Fig. 4I-K), and MMP2, IL-1β, TNF-α (Fig. 4O-Q). Based on the aforementioned results, it can be concluded that Sirt2 can delay H_2O_2-induced senescence in primary VSMCs.

Sirt2 regulates VSMC senescence and delays the formation of VPs via the AMPK/FOXO3a pathway

The AMPK/FOXO3a pathway is one of the important downstream pathways of Sirt2 [5]. Previous studies have indicated that Sirt2 can promote the activation of the AMPK pathway by deacetylating liver kinase B1 (LKB1), thereby reversing aging-associated pathological cardiac hypertrophy [8]. Therefore, we further investigated the effect of Sirt2 on the AMPK/FOXO3a.

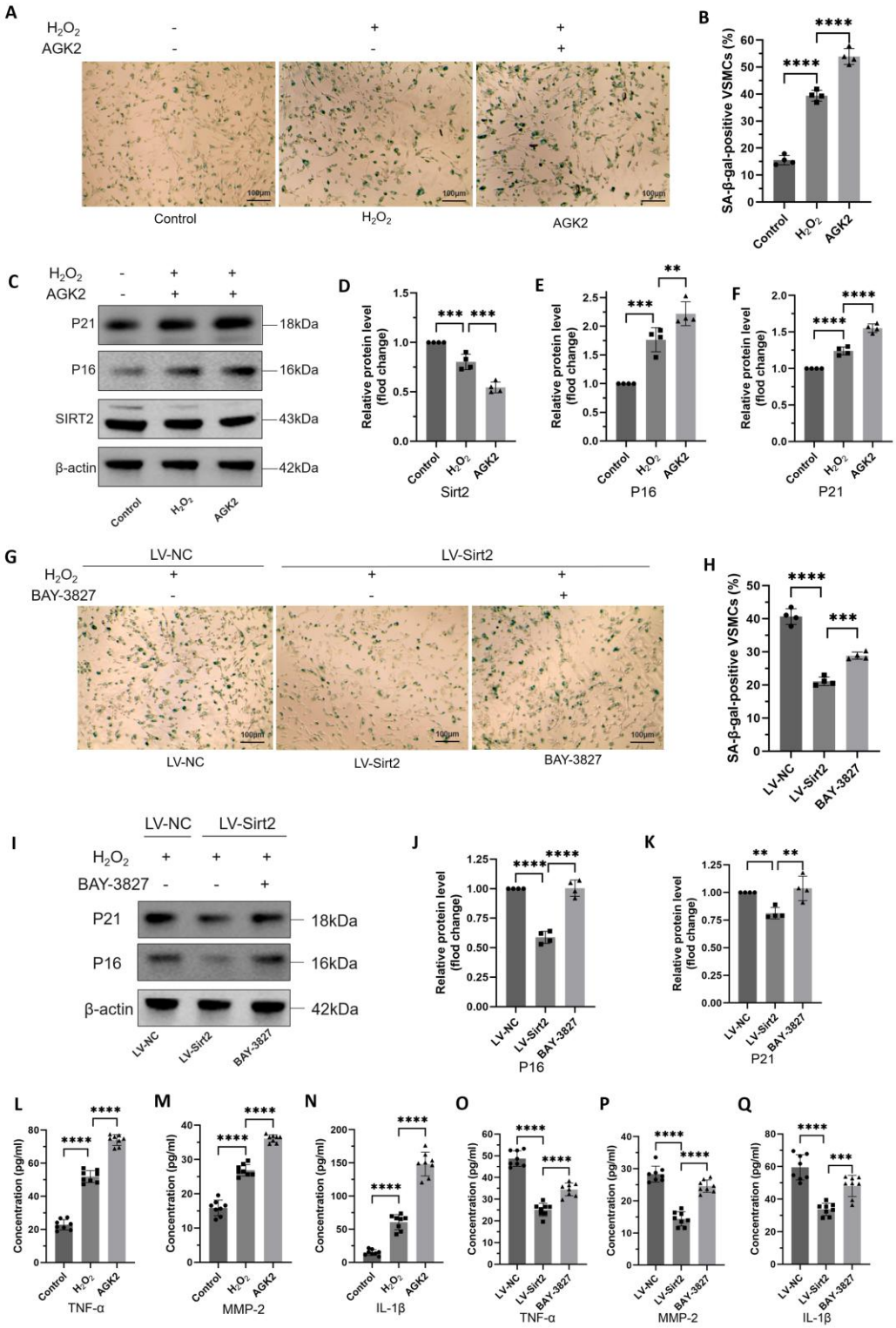

Figure 4. Effect of Sirt2 on senescence in primary VSMCs. (A, G) Representative SA-β-gal staining images from the indicated groups. Scale bar = 100 μm. n=4 per group. B, H: Quantification of senescent VSMCs. **(C, I)** Western blot analysis of Sirt2, P16, P21, and β-actin. n=4 per group. D-F, J-K: Quantification of Sirt2 (D), P16 (E, J), and P21 (F, K) expression normalized to β-actin. Data are normalized to the Control group (D-F) and LV-NC group (J-K) (set to 1). **(L-Q)** ELISA quantification of TNF-α (L, O), MMP-2 (M, P), and IL-1β (N, Q) levels. n=8 per group. All data were analyzed by one-way ANOVA with Holm-Šídák's post hoc test. Note: ns: not significant; **P*< 0.05; ***P*< 0.01; ****P*< 0.001; *****P*< 0.0001.

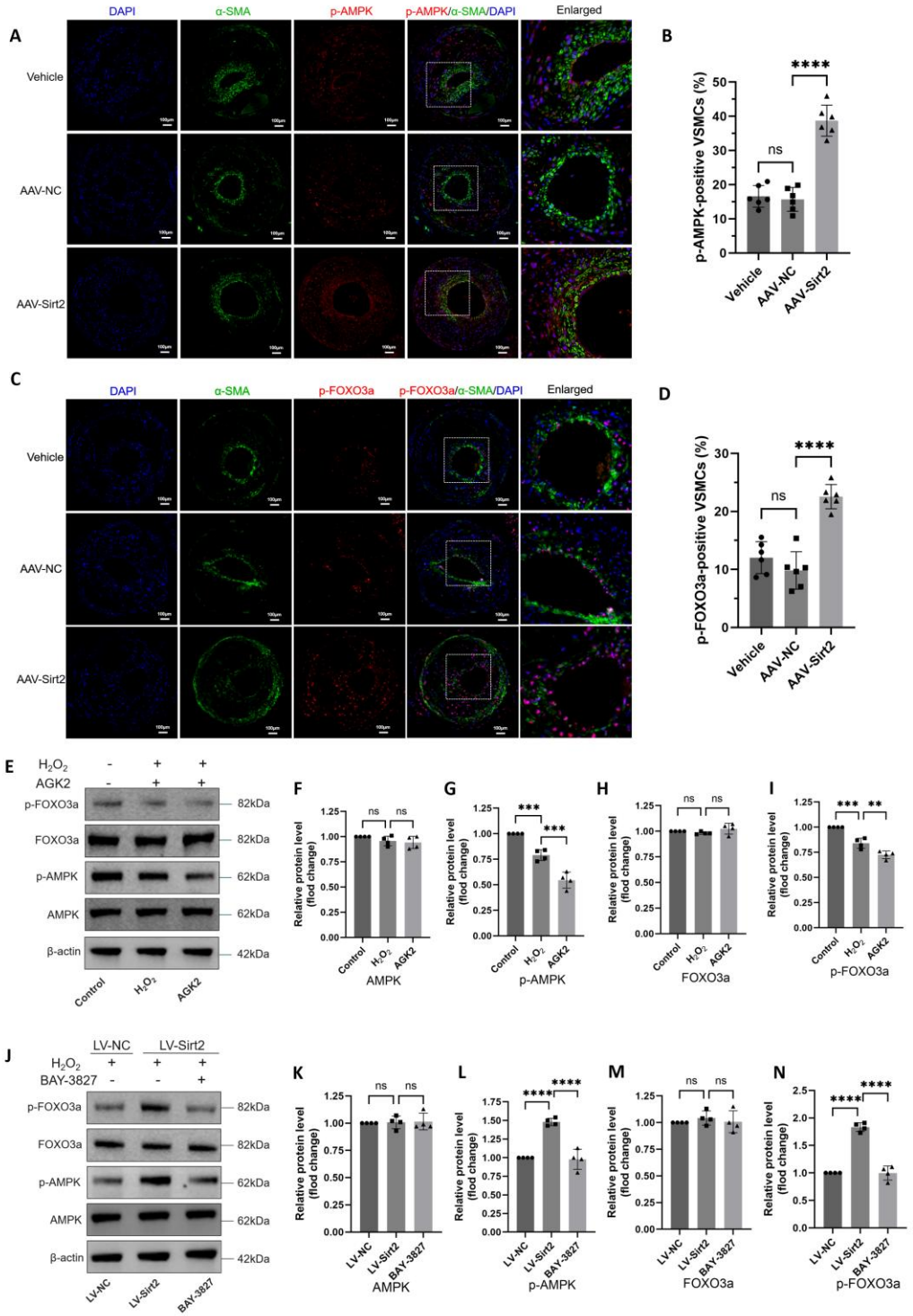

Figure 5. Sirt2 Regulates VSMC Senescence and Delays Vulnerable Plaque Formation via the AMPK/FOXO3a Pathway. (A, C) Representative immunofluorescence images showing p-AMPK (A) or p-FOXO3a (C) (red) co-localization with α-SMA (green) in mouse carotid arteries. Arrows indicate p-AMPK or p-FOXO3a-positive VSMCs. Scale bar = 100 μm. n=6 per group. B, D: Quantification of p-AMPK (B) and p-FOXO3a (D) expression in VSMCs. E, J: Western blot analysis of AMPK, p-AMPK, FOXO3a, p-FOXO3a, and β-actin in the indicated groups. n=4 per group. **(F-I, K-N)** Quantification of total AMPK (F, K), p-AMPK (G, L), total FOXO3a (H, M), and p-FOXO3a (I, N) expression normalized to β-actin. Data are normalized to the Control group (F-I) and LV-NC group (K-N) (set to 1). All data were analyzed by one-way ANOVA with Holm-Šídák's post hoc test. Note: ns: not significant; **P*< 0.05; ***P*< 0.01; ****P*< 0.001; *****P*< 0.0001.

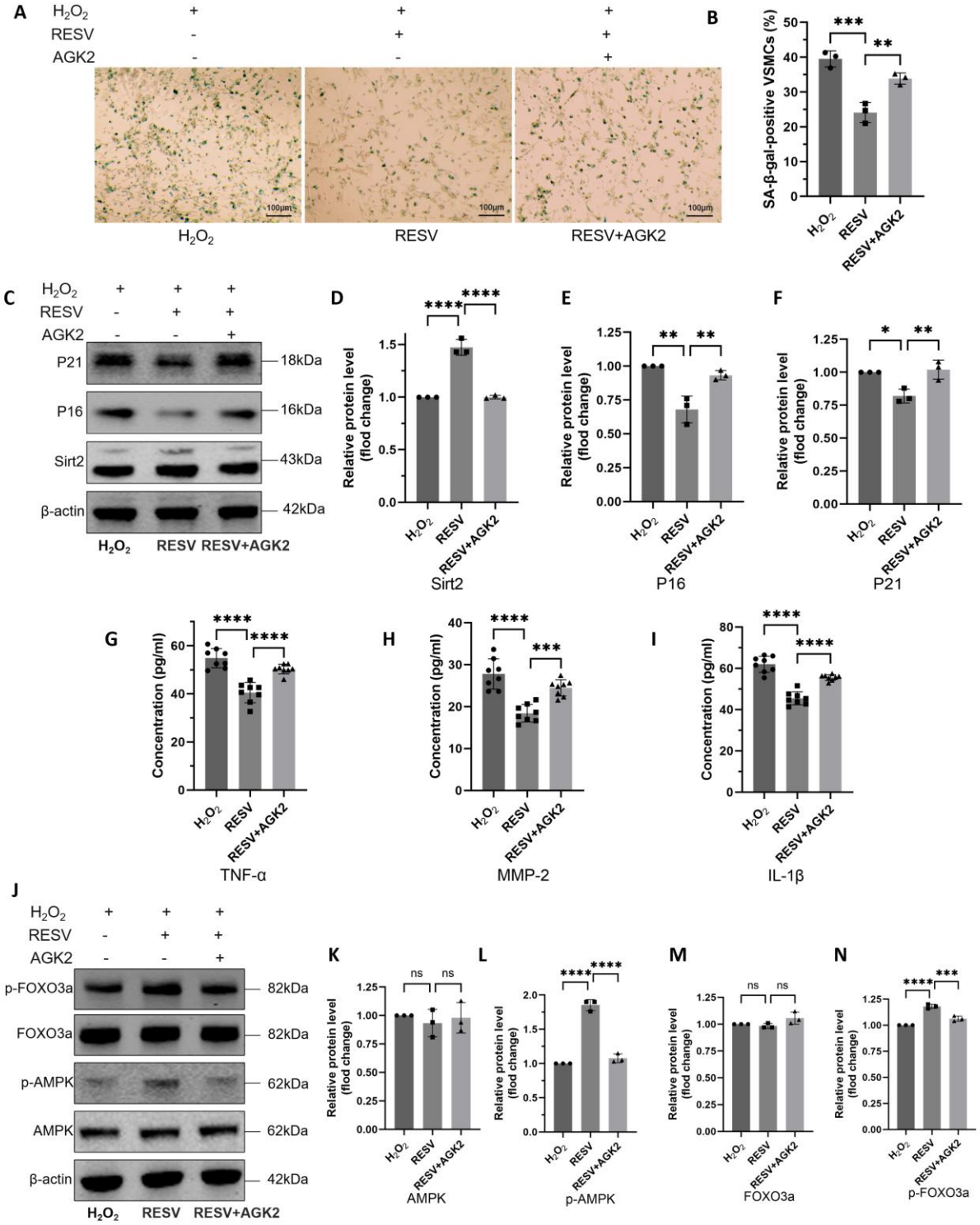

Figure 6. Resveratrol alleviates VSMC senescence in a Sirt2-dependent manner. (A) Representative SA-β-gal staining images from the indicated groups. Scale bar = 100 μm. n=3 per group. B: Quantification of senescent VSMCs. C: Western blot analysis of Sirt2, P16, P21, and β-actin. n=3 per group. **(D-F)** Quantification of Sirt2 (D), P16 (E), and P21 (F) expression normalized to β-actin. Data are normalized to the H2O2 group. G-I: ELISA quantification of TNF-α (G), MMP-2 (H), and IL-1β (I) levels. n=8 per group. **(J)** Western blot analysis of AMPK, p-AMPK, FOXO3a, p-FOXO3a, and β-actin. n=3 per group. **(K-N)** Quantification of total AMPK (K), p-AMPK (L), total FOXO3a (M), and p-FOXO3a (N) expression normalized to β-actin. Data are normalized to the H2O2 group (set to 1). All data were analyzed by one-way ANOVA with Holm-Šídák's post hoc test. Note: ns: not significant; *P< 0.05; **P< 0.01; ***P< 0.001; ****P< 0.0001.

In vivo, we detected the phosphorylation levels of AMPK and FOXO3a using immunofluorescence double staining. The results demonstrated that VSMC-specific overexpression of Sirt2 in VPs significantly increased the phosphorylation levels of both AMPK and FOXO3a within VSMCs (Fig. 5A-D).

In vitro, after inducing VSMC senescence with H_2O_2, the expression levels of AMPK and FOXO3a did not change significantly (Fig. 5E, F, H). However, their phosphorylation levels were significantly reduced compared to the control group. Treatment with the specific Sirt2 inhibitor AGK2 further decreased the phosphorylation levels of AMPK and FOXO3a (Fig. 5E, G I). After overexpression of Sirt2, the expression levels of AMPK and FOXO3a showed no significant changes, while their phosphorylation levels were significantly increased (Fig. 5J-N).

These results suggest that the AMPK/FOXO3a pathway may be involved in the process of Sirt2 regulating VSMC senescence and delaying VP formation. Subsequently, based on the overexpression of Sirt2 in VSMCs, we employed the AMPK-specific inhibitor BAY-3827 to suppress AMPK activity, thereby further validating the role of the AMPK/FOXO3a pathway in Sirt2-mediated attenuation of VSMC senescence and inhibition of VPs formation.

In VSMCs overexpressing Sirt2, AMPK inhibition reversed the anti-senescent effect of Sirt2. Compared with the LV-Sirt2 group, the BAY-3827 group showed no significant difference in the expression levels of AMPK and FOXO3a, while their phosphorylation levels were decreased (Fig. 5J-N). We further examined the senescence of VSMCs. The results showed that compared with the LV-Sirt2 group, the BAY-3827 group exhibited a significant increase in the number of senescent VSMCs (Fig. 4G-H), as well as in the levels of $P16^{INK4A}$, P21 (Fig. 4I-K), and the SASP factors (MMP2, IL-1β, and TNF-α) (Fig. 4O-Q). In conclusion, our findings suggest that Sirt2 regulates VSMC senescence and delays the formation of VPs through a mechanism involving the AMPK/FOXO3a pathway.

Resveratrol alleviates VSMC senescence in a Sirt2-dependent manner

Previous studies have shown that resveratrol delays atherosclerosis progression by upregulating Sirt2 in endothelial cells [15]; however, its role in VSMC senescence and the underlying mechanism remain unclear. To address this, we treated H_2O_2-induced senescent VSMCs with resveratrol and further used the Sirt2-specific inhibitor AGK2 to validate the involvement of Sirt2.

We observed that compared to the H_2O_2 group, the RESV group exhibited significantly increased Sirt2 protein levels (Fig. 6C-D) and enhanced phosphorylation of AMPK and FOXO3a (Fig. 6J-N), accompanied by a marked reduction in the number of senescent VSMCs (Fig. 6A-B), decreased expression of senescence markers P16 and P21 (Fig. 6C-F), and lower levels of MMP2, IL-1β, and TNF-α (Fig. 6G-I). However, these protective effects of resveratrol were partially reversed upon Sirt2 inhibition with AGK2. Specifically, compared to the RESV group, the RESV+AGK2 group showed significantly decreased Sirt2 protein levels (Fig. 6C-D) and reduced AMPK and FOXO3a phosphorylation, along with an increased number of senescent VSMCs (Fig. 6A-B), elevated expression of P16 and P21 (Fig. 6C-F), and higher levels of MMP2, IL-1β, and TNF-α (Fig. 6G-I). These results indicate that resveratrol delays VSMC senescence via the Sirt2-AMPK-FOXO3a axis, providing a potential therapeutic strategy targeting Sirt2.

DISCUSSION

ACS is one of the leading causes of acute cardiovascular mortality, and its pathophysiological basis lies in the rupture of vulnerable plaques (VPs) [1, 2]. Therefore, investigating the formation, progression, and underlying mechanisms of VPs plays a crucial role in preventing the occurrence of ACS. Vascular smooth muscle cells (VSMCs) and their derivatives serve as the primary sources of both cells and ECM within atherosclerotic plaques. However, senescent VSMCs undergo a SASP shift, leading to the release of large amounts of pro-inflammatory cytokines (such as IL-6 and IL-1), chemokines (such as IL-8), CXC chemokine ligand 1 (CXCL1), and proteases, including matrix metalloproteinases (MMPs) [16]. This shift in VSMCs further exacerbates inflammatory responses within atherosclerotic plaques and promotes the degradation of the ECM, ultimately leading to reduced plaque stability. However, the specific mechanisms driving VSMC senescence remain to be fully elucidated. Although previous studies have implicated Sirt2 in the progression of atherosclerotic plaques, most of this research has primarily focused on macrophages and vascular endothelial cells [15, 17, 18]. Therefore, whether there is a correlation between Sirt2 and the senescence of VSMCs, as well as its potential influence on the formation of VPs, still requires further investigation.

In this study, we demonstrated that Sirt2 significantly increased the fibrous cap area, enhanced collagen content, and reduced lipid infiltration within atherosclerotic plaques. Furthermore, Sirt2 markedly attenuated both *in vivo* and *in vitro* VSMC senescence, thereby promoting plaque stability. Finally, we further confirmed the role of

the AMPK-FOXO3a signaling pathway in mediating the effects of Sirt2 on VSMC senescence and vulnerable plaque formation. Thus, we have provided evidence for a mechanism by which the Sirt2-AMPK-FOXO3a signaling axis regulates VSMC senescence and delays the formation of VPs, offering novel insights for the prevention and treatment of ACS (Fig. 7).

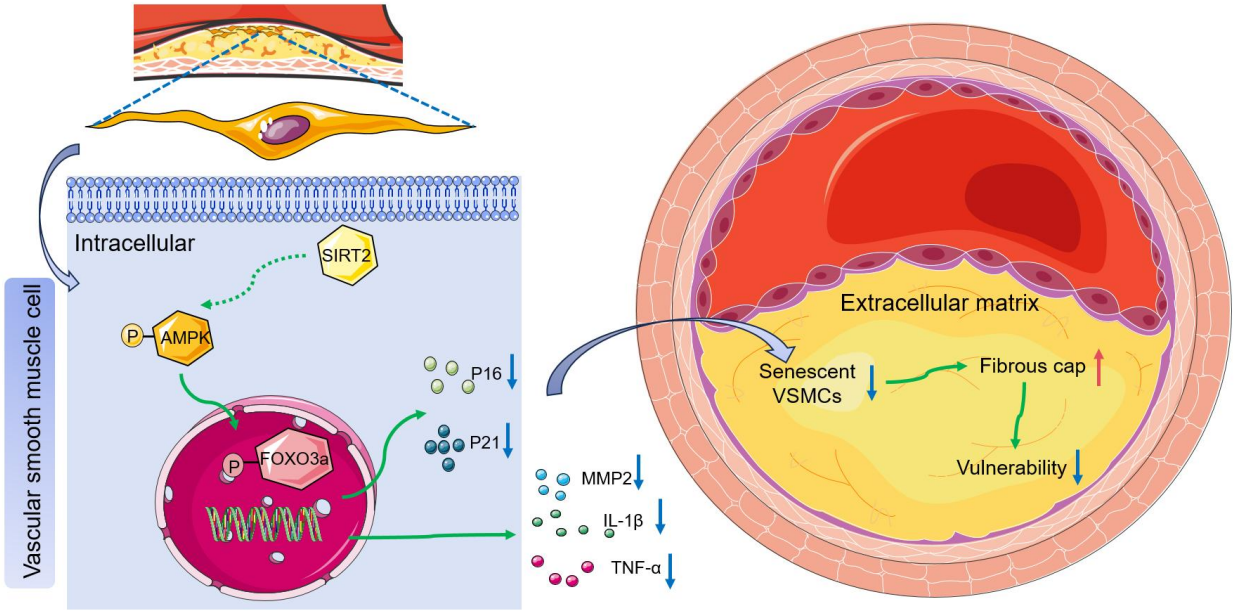

Figure 7. Schematic diagram illustrating the proposed mechanism by which Sirt2 regulates vascular smooth muscle cell senescence to delay the formation of VPs. Overexpression of Sirt2 is associated with increased phosphorylation of AMPK-FOXO3a, suggesting activation of the AMPK-FOXO3a pathway, which in turn delays VSMC senescence and thereby enhances plaque stability.

Currently, seven homologs of sirtuins (SIRTs) have been identified in mammals [19]. Research linking SIRTs to aging dates back more than two decades, with studies showing that overexpression of Sir2 (a member of the sirtuin family) in yeast can significantly extend its lifespan [20]. Subsequently, further research has revealed the role of sirtuins in extending the lifespan of *Caenorhabditis elegans*, *Drosophila*, and mice [21, 22]. The occurrence of cardiovascular diseases is closely associated with aging [23]. While numerous studies have revealed the roles of Sirt1, Sirt3, and Sirt6 in cardiovascular diseases, research on Sirt2, which has the highest basal expression in the human aorta, remains quite limited in the context of cardiovascular diseases and vascular aging [7]. Zhang et al. demonstrated that Sirt2 can delay the progression of atherosclerosis by suppressing the polarization of macrophages toward the M1 phenotype in LDLr-/- mice [17]. However, this study did not further investigate the specific mechanisms by which Sirt2 regulates macrophages and also lacked validation through *in vitro*. Zhang et al. demonstrated that Sirt2 deficiency promotes aging-induced vascular remodeling by modulating p66Shc, suggesting that dysregulation of Sirt2 is associated with human vascular aging and related diseases [6]. These findings collectively underscore the role of Sirt2 in vascular aging and atherosclerosis. Building on prior research, our work further investigates the mechanism of Sirt2 in regulating VSMC senescence and VP formation through overexpression or inhibition of Sirt2, providing a new potential target for delaying the progression of VPs.

Notably, an analysis of a public proteomic dataset comprising 4,263 individuals aged 18 to 95 years revealed that plasma Sirt2 levels are negatively correlated with age, indicating that decreased Sirt2 levels may serve as a significant risk factor for age-related diseases [6, 24].This finding, together with the conserved high expression of SIRT2 in both human and mouse aortas [6], provides supportive—though not direct—evidence for the clinical relevance of our findings. In conjunction with the protective role of Sirt2 observed in this study, these observations raise the possibility that maintaining Sirt2 expression could represent a potential therapeutic strategy for delaying VPs progression.

Currently, research on interventional drugs targeting Sirt2 for cardiovascular diseases has made preliminary progress. Sun et al. found that in a mouse model of dilated cardiomyopathy, colchicine could upregulate Sirt2, leading to the deacetylation and inactivation of NLRP3, reducing neutrophil infiltration and levels of

inflammatory cytokines, thereby improving cardiac function [25]. Wu et al. demonstrated that simvastatin could alleviate hypoxemia, inflammatory response, mean pulmonary arterial pressure, and right ventricular systolic pressure in rats with acute pulmonary embolism via the Sirt2/NF-κB pathway, thus playing a role in preventing pulmonary hypertension [26]. Resveratrol, a natural polyphenol compound, exhibits various cardiovascular protective functions such as anti-aging, antioxidant, and anti-inflammatory effects [27]. Yu et al. demonstrated that resveratrol can upregulate Sirt2 expression and inhibit TNF-α-induced oxidative stress in human umbilical vein endothelial cells (HUVECs), thereby slowing the progression of atherosclerosis [15]. Additionally, Jin et al. demonstrated that resveratrol can enhance AMPK activity, increase Sirt1 expression in the thoracic aorta of aged mice, and delay Ang II-induced senescence in VSMCs [28]. These findings collectively suggest the potential role of resveratrol in regulating Sirt2, AMPK, VSMC senescence, and atherosclerosis. However, the specific mechanisms through which resveratrol modulates Sirt2-mediated VSMC senescence and atherosclerosis still require further investigation. In this study, using the H_2O_2-induced VSMC senescence model, we found that resveratrol inhibits VSMC senescence via the Sirt2-AMPK-FOXO3a signaling pathway, providing a new therapeutic perspective for delaying the formation of VPs. However, current research on cardiovascular drugs targeting Sirt2 remains insufficient, and systematic in-depth exploration is still needed in areas such as atherosclerosis.

AMPK plays a critical role in cellular energy homeostasis, and numerous studies have revealed the relationship between AMPK and cardiovascular aging [29]. Previous research has shown that metformin modulates biological aging by activating the AMPK pathway, thereby improving patient survival rates [30]. Furthermore, AMPK can cooperate with sirtuins to regulate aging-related cardiovascular diseases. Chen et al. demonstrated that inhibiting dipeptidyl peptidase-4 (DPP4) ameliorates endothelial senescence by activating the AMPK/SIRT1/Nrf2 signaling pathway [31]. Tang et al. found that Sirt2 maintains AMPK activity in aging-induced hypertrophic hearts, and loss of Sirt2 leads to decreased AMPK activity, exacerbating aging-associated myocardial hypertrophy [8]. The aforementioned studies have all revealed the anti-aging role of AMPK in cardiovascular diseases. However, the roles of Sirt2, AMPK, and their downstream pathways in VSMC senescence require further exploration. This study elucidates the mechanism by which Sirt2 regulates VSMC senescence and delays VP formation through activation of the AMPK-FOXO3a axis.

FOXO3a is an important member of the forkhead box O (FOXO) transcription factor superfamily and plays a critical role in regulating various pathophysiological processes, including apoptosis, proliferation, autophagy, and aging [32]. Recent studies have shown that FOXO3a is also involved in the regulation of vascular aging. For instance, Yan et al. reported that FOXO3 delays the senescence of human MSCs by enhancing the self-renewal potential of human vascular endothelial cells (HVECs) and VSMCs, thereby exerting an anti-vascular aging effect [33]. The subcellular localization and transcriptional activity of FOXO3a are precisely regulated by various post-translational modifications (PTMs) [34]. Among these, AMPK directly phosphorylates FOXO3a, promoting its translocation from the cytoplasm to the nucleus, thereby contributing to the maintenance of cellular energy homeostasis [35]. In this study, immunofluorescence double staining revealed that phosphorylated FOXO3a (p-FOXO3a) was primarily localized in the nucleus (as evidenced by the co-localization of red and blue fluorescence), a finding consistent with previous reports. Taken together, our results suggest that Sirt2 overexpression upregulates AMPK phosphorylation, and activated AMPK subsequently promotes FOXO3a phosphorylation and its nuclear translocation, thereby exerting a protective effect against VSMC senescence (Fig. 7).

However, this study still has certain limitations. First, while our in vitro and in vivo experiments support a protective role for SIRT2 in VSMC senescence and vulnerable plaque formation, direct validation in human vulnerable plaque tissues is lacking. Publicly available datasets on human atherosclerosis generally do not provide the detailed plaque phenotype information needed to specifically validate findings related to plaque vulnerability. As such, the GTEx and plasma proteomic data we cite serve as supportive—rather than definitive—evidence. Future studies utilizing well-characterized human carotid endarterectomy samples will be important to address this limitation. Second, the sample size of n=6 per group in our animal study, while consistent with exploratory studies in this field, may limit the power to detect smaller effects. However, all key differences observed between AAV-NC and AAV-Sirt2 groups were highly significant with effect sizes far exceeding the minimum detectable threshold for this sample size. Thus, our major conclusions remain robust. Future studies with larger cohorts are warranted to validate these findings and explore subtler effects. Additionally, we observed that Sirt2 inhibits VSMC senescence by regulating the phosphorylation levels of AMPK. However, as a classic energy sensor, AMPK is typically activated via phosphorylation at Thr172 by kinases such as LKB1. The study by Tang et al. also indicates that Sirt2 activates

AMPK precisely through deacetylating LKB1 [8]. This suggests that the regulatory effect of Sirt2 on AMPK observed in our study is likely indirect, potentially mediated through intermediate molecules like LKB1. Therefore, whether Sirt2 can directly regulate AMPK phosphorylation, and whether other unknown regulatory factors exist between them, still requires further experimental investigation.

In conclusion, this study identifies a role for Sirt2 in regulating VSMC senescence and vulnerable plaque formation, potentially via the AMPK-FOXO3a pathway. Furthermore, using resveratrol, we provide pharmacological evidence that targeting Sirt2 attenuates VSMC senescence in a Sirt2-dependent manner. This study not only identifies Sirt2 as a key regulator of VSMC senescence but also highlights its potential as a novel therapeutic target for delaying VPs progression, offering new insights for the prevention and treatment of ACS.

Acknowledgements

The study received funding from the National Natural Science Foundations of China (NSFC, Grant No. 82271605, 82471603, 82071573).

Conflicts of interest

We have no conflicts of interest.

Data and materials availability

All initial data from this study are available by e-mail to the corresponding author upon reasonable request.

Supplementary Materials

The Supplementary data are available online at: www.aginganddisease.org/EN/10.14336/AD.2026.0063.

References

[1] Bergmark BA, Mathenge N, Merlini PA, Lawrence-Wright MB, Giugliano RP (2022). Acute coronary syndromes. Lancet, 399:1347–1358.

[2] Gaba P, Gersh BJ, Muller J, Narula J, Stone GW (2023). Evolving concepts of the vulnerable atherosclerotic plaque and the vulnerable patient: implications for patient care and future research. Nat Rev Cardiol, 20:181–196.

[3] Dawson LP, Lum M, Nerleker N, Nicholls SJ, Layland J (2022). Coronary Atherosclerotic Plaque Regression: JACC State-of-the-Art Review. J Am Coll Cardiol, 79:66–82.

[4] Grootaert MOJ, Bennett MR (2021). Vascular smooth muscle cells in atherosclerosis: time for a re-assessment. Cardiovascular Research, 117:2326–2339.

[5] Wu B, You S, Qian H, Wu S, Lu S, Zhang Y, et al. (2021). The role of SIRT2 in vascular-related and heart-related diseases: A review. J Cellular Molecular Medi, 25:6470–6478.

[6] Zhang Y, Wang X, Li X-K, Lv S-J, Wang H-P, Liu Y, et al. (2023). Sirtuin 2 deficiency aggravates ageing-induced vascular remodelling in humans and mice. European Heart Journal, 44:2746–2759.

[7] Puspitasari YM (2023). Sirtuin 2 in vascular ageing: the forsaken child? European Heart Journal, 44:2760–2762.

[8] Tang X, Chen X-F, Wang N-Y, Wang X-M, Liang S-T, Zheng W, et al. (2017). SIRT2 Acts as a Cardioprotective Deacetylase in Pathological Cardiac Hypertrophy. Circulation, 136:2051–2067.

[9] Ye Y, Yang K, Liu H, Yu Y, Song M, Huang D, et al. (2023). SIRT2 counteracts primate cardiac aging via deacetylation of STAT3 that silences CDKN2B. Nat Aging, 3:1269–1287.

[10] Steinberg GR, Hardie DG (2023). New insights into activation and function of the AMPK. Nat Rev Mol Cell Biol, 24:255–272.

[11] Cao G, Lin M, Gu W, Su Z, Duan Y, Song W, et al. (2023). The rules and regulatory mechanisms of FOXO3 on inflammation, metabolism, cell death and aging in hosts. Life Sci, 328:121877.

[12] Xia W, Zhang F, Xie C, Jiang M, Hou M (2015). Macrophage migration inhibitory factor confers resistance to senescence through CD74-dependent AMPK-FOXO3a signaling in mesenchymal stem cells. Stem Cell Res Ther, 6:82.

[13] Brito PM, Devillard R, Nègre-Salvayre A, Almeida LM, Dinis TCP, Salvayre R, et al. (2009). Resveratrol inhibits the mTOR mitogenic signaling evoked by oxidized LDL in smooth muscle cells. Atherosclerosis, 205:126–134.

[14] Zhu Y, Takayama T, Wang B, Kent A, Zhang M, Binder BYK, et al. (2017). Restenosis Inhibition and Re-differentiation of TGFβ/Smad3-activated Smooth Muscle Cells by Resveratrol. Sci Rep, 7:41916.

[15] Yu H, Pan W, Huang H, Chen J, Sun B, Yang L, et al. (2019). Screening Analysis of Sirtuins Family Expression on Anti-Inflammation of Resveratrol in Endothelial Cells. Med Sci Monit, 25:4137–4148.

[16] Basatemur GL, Jørgensen HF, Clarke MCH, Bennett MR, Mallat Z (2019). Vascular smooth muscle cells in atherosclerosis. Nat Rev Cardiol, 16:727–744.

[17] Zhang B, Ma Y, Xiang C (2018). SIRT2 decreases atherosclerotic plaque formation in low-density lipoprotein receptor-deficient mice by modulating macrophage polarization. Biomed Pharmacother, 97:1238–1242.

[18] Liu Q-Q, Ren K, Liu S-H, Li W-M, Huang C-J, Yang X-H (2019). MicroRNA-140-5p aggravates hypertension and oxidative stress of atherosclerosis via targeting Nrf2 and Sirt2. Int J Mol Med, 43:839–849.

[19] Zhao L, Cao J, Hu K, He X, Yun D, Tong T, et al. (2020). Sirtuins and their Biological Relevance in Aging and Age-Related Diseases. Aging Dis, 11:927–945.

[20] Kaeberlein M, McVey M, Guarente L (1999). The SIR2/3/4 complex and SIR2 alone promote longevity in Saccharomyces cerevisiae by two different mechanisms. Genes Dev, 13:2570–2580.

[21] Burnett C, Valentini S, Cabreiro F, Goss M, Somogyvári M, Piper MD, et al. (2011). Absence of effects of Sir2 overexpression on lifespan in C. elegans and Drosophila. Nature, 477:482–485.

[22] Kanfi Y, Naiman S, Amir G, Peshti V, Zinman G, Nahum L, et al. (2012). The sirtuin SIRT6 regulates lifespan in male mice. Nature, 483:218–221.

[23] Liberale L, Badimon L, Montecucco F, Lüscher TF, Libby P, Camici GG (2022). Inflammation, Aging, and Cardiovascular Disease: JACC Review Topic of the Week. J Am Coll Cardiol, 79:837–847.

[24] Lehallier B, Gate D, Schaum N, Nanasi T, Lee SE, Yousef H, et al. (2019). Undulating changes in human plasma proteome profiles across the lifespan. Nat Med, 25:1843–1850.

[25] Sun X, Duan J, Gong C, Feng Y, Hu J, Gu R, et al. (2022). Colchicine Ameliorates Dilated Cardiomyopathy Via SIRT2-Mediated Suppression of NLRP3 Inflammasome Activation. J Am Heart Assoc, 11:e025266.

[26] Wu Z-Y, Li H, Tang Y-J (2018). Effect of simvastatin on the SIRT2/NF-κB pathway in rats with acute pulmonary embolism. Pharm Biol, 56:511–518.

[27] Ren Z-Q, Zheng S-Y, Sun Z, Luo Y, Wang Y-T, Yi P, et al. (2025). Resveratrol: Molecular Mechanisms, Health Benefits, and Potential Adverse Effects. MedComm (2020), 6:e70252.

[28] Kim EN, Kim MY, Lim JH, Kim Y, Shin SJ, Park CW, et al. (2018). The protective effect of resveratrol on vascular aging by modulation of the renin-angiotensin system. Atherosclerosis, 270:123–131.

[29] Barcena ML, Aslam M, Norman K, Ott C, Ladilov Y (2024). Role of AMPK and Sirtuins in Aging Heart: Basic and Translational Aspects. Aging Dis, 16:3335–3360.

[30] Hamczyk MR, Nevado RM, Barettino A, Fuster V, Andrés V (2020). Biological Versus Chronological Aging: JACC Focus Seminar. J Am Coll Cardiol, 75:919–930.

[31] Chen Z, Yu J, Fu M, Dong R, Yang Y, Luo J, et al. (2020). Dipeptidyl peptidase-4 inhibition improves endothelial senescence by activating AMPK/SIRT1/Nrf2 signaling pathway. Biochem Pharmacol, 177:113951.

[32] Hao X-D, Liu J-X, Zhang J-S (2024). Longevity factor FOXO3a: A potential therapeutic target for age-related ocular diseases. Life Sci, 350:122769.

[33] Yan P, Li Q, Wang L, Lu P, Suzuki K, Liu Z, et al. (2019). FOXO3-Engineered Human ESC-Derived Vascular Cells Promote Vascular Protection and Regeneration. Cell Stem Cell, 24:447-461.e8.

[34] Ma X, Lin Y, Zhang L, Huang Z, Zhang Y, Fu X, et al. (2025). The dual missions of FoxO3a in inflammatory diseases: Regulation of antioxidant enzymes and involvement in programmed cell death. Int Immunopharmacol, 151:114369.

[35] Peserico A, Chiacchiera F, Grossi V, Matrone A, Latorre D, Simonatto M, et al. (2013). A novel AMPK-dependent FoxO3A-SIRT3 intramitochondrial complex sensing glucose levels. Cell Mol Life Sci, 70:2015–2029.